KURENAI
Kyoto University Research Information Repository

KYOTO UNIVERSITY

Title	Crystal structure of a thermophilic GrpE protein: insight into thermosensing function for the DnaK chaperone system
Author(s)	Nakamura, Akira; Takumi, Kouhei; Miki, Kunio
Citation	Journal of molecular biology (2010), 396(4): 1000-1011
Issue Date	2010-03-05
URL	http://hdl.handle.net/2433/132547
Right	© 2009 Elsevier Ltd
Type	Journal Article
Textversion	author

Kyoto University

Title

Crystal structure of a thermophilic GrpE protein: Insight into thermosensing function for the

DnaK chaperone system

Running title

Structural basis of a thermosensor GrpE

Authors

Akira Nakamura[1], Kouhei Takumi[1], and Kunio Miki[1,2*]

Affiliations

[1]Department of Chemistry, Graduate School of Science, Kyoto University, Sakyo-ku, Kyoto

606-8502, Japan, [2]RIKEN SPring-8 Center at Harima Institute, Koto 1-1-1, Sayo, Hyogo

679-5148, Japan

Corresponding author

*Correspondence should be addressed to Kunio Miki.

Tel: +81-75-753-4029; Fax: +81-75-753-4032; e-mail: miki@kuchem.kyoto-u.ac.jp

Postal Address: Department of Chemistry, Graduate School of Science, Kyoto University,

Sakyo-ku, Kyoto 606-8502, Japan

Abstract

A homodimeric GrpE protein functions as a nucleotide exchange factor of the eubacterium DnaK molecular chaperone system. The co-chaperone GrpE accelerates ADP dissociation from, and promotes ATP binding to, DnaK, which cooperatively facilitates the DnaK chaperone cycle with another co-chaperone, DnaJ. GrpE characteristically undergoes two-step conformational changes in response to elevation of the environmental temperature. In the first transition at heat-shock temperatures, fully reversible and functionally deficient structural alteration takes place in GrpE, and then the higher temperatures lead to irreversible dissociation of the GrpE dimer into monomers as the second transition. GrpE is also thought to be a thermosensor of the DnaK system, since it is the only member of the DnaK system that changes its structure reversibly and loses its function at heat-shock temperatures of various organisms. We here report the crystal structure of GrpE from *Thermus thermophilus* HB8 (GrpE$_{Tth}$) at 3.23 Å resolution. The resolved structure is compared with that of GrpE from mesophilic *Escherichia coli* (GrpE$_{Eco}$), revealing structural similarities, particularly in the DnaK interaction regions, and structural characteristics for the thermal stability of GrpE$_{Tth}$. In addition, the structure analysis raised the possibility that the polypeptide chain in the reported GrpE$_{Eco}$ structure was misinterpreted. Comparison of these two GrpE structures combined with the results of limited proteolysis experiments provide insight into the protein dynamics of GrpE$_{Tth}$ correlated with the shift of temperature, and also suggest that the

localized and partial unfolding at the plausible DnaK interaction sites of GrpE$_{Tth}$ causes

functional deficiency of nucleotide exchange factor in response to the heat shock.

Keywords

unfolding, heat-shock response, thermosensor, thermal stability, protein dynamics

Abbreviations

nucleotide exchange factor, NEF

DnaK from *Escherichia coli*, DnaK$_{Eco}$

GrpE from *Escherichia coli*, GrpE$_{Eco}$

nucleotide-binding domain, NBD

differential scanning calorimetry, DSC

GrpE from *Thermus thermophilus* HB8, GrpE$_{Tth}$

DnaK from *Thermus thermophilus* HB8, DnaK$_{Tth}$

single-wavelength anomalous dispersion, SAD

metalloendopeptidase, MEP

matrix-assisted laser desorption/ionization, MALDI

mass spectrometry, MS

Introduction

Molecular chaperone proteins are involved in various cellular functions, such as protein folding, refolding/degradation of nonnative proteins, prevention of protein aggregation under stress conditions, regulation of protein activities, and so on.[1] Hsp70 is a ubiquitous molecular chaperone family found in eubacteria, eukarya, and some archaea. Hsp70-family proteins play important roles in the maintenance of protein quality, including folding of nascent polypeptides, transmembrane transport of proteins, and suppression of protein aggregation.[2] Hsp70 is an ATP-dependent molecular chaperone protein that exhibits weak intrinsic ATPase activity, and it is usually present in an ATP-bound state. Although Hsp70 has low affinity with fast exchange rates for substrates in its ATP-bound state, ADP-bound Hsp70 undergoes an internal conformational change that results in comparatively high affinity with slow exchange rates for substrates.[3] This structural alteration of Hsp70 is coupled to ATP hydrolysis and ADP/ATP exchange, which is closely related to the actions of the co-chaperones, J-protein (Hsp40) and nucleotide exchange factor (NEF).[3] Both cooperative proteins are essential for efficient progression of the Hsp70 chaperone cycle.

In prokaryotes, DnaK of *Escherichia coli* (DnaK$_{Eco}$) is a well-known Hsp70 homologue whose ATPase activity is facilitated by an Hsp40 homologue DnaJ in synergy with substrate binding.[2] ADP dissociation from DnaK$_{Eco}$ is accelerated 5000-fold by an NEF, GrpE,[4] resulting in efficient ATP rebinding to and substrate release from DnaK.[5] These three proteins

constitute the DnaK chaperone system. The crystal structure revealed a direct interaction between the homodimeric GrpE from *E. coli* (GrpE$_{Eco}$) and the nucleotide-binding domain of DnaK$_{Eco}$,[6] suggesting a forced opening of the nucleotide-binding cleft of DnaK$_{Eco}$ by insertion of the β-sheet domain of GrpE$_{Eco}$. Interestingly, the results of the CD measurement and differential scanning calorimetry (DSC) indicated that GrpE$_{Eco}$ is the only component of the DnaK$_{Eco}$ system that undergoes temperature-dependent conformational changes in the physiologically relevant temperature range, exhibiting two distinctive thermal transitions with midpoints at ~48°C and 75-80°C.[7] Conformational changes of GrpE$_{Eco}$ at the lower-temperature transition are fully reversible, and its NEF activity reaches a maximum at 40°C,[7] while the second transition represents irreversible inactivation of GrpE$_{Eco}$. Thus, GrpE$_{Eco}$ becomes transiently unable to interact with the nucleotide-binding domain of DnaK$_{Eco}$ at heat-shock temperatures, resulting in stabilization of the DnaK-ADP-substrate complex. GrpE is therefore thought to act as a thermosensor of the DnaK system that prevents substrate proteins from thermal denaturation.[8]

In addition to GrpE$_{Eco}$, GrpE of the thermophilic eubacterium *Thermus thermophilus* HB8 (GrpE$_{Tth}$) has been well characterized, revealing that the two GrpE show similar biochemical and biophysical properties.[9] The amino acid sequence alignment and CD spectra indicated that these two GrpE proteins probably have common structural features, including the domain composition, i.e., the N-terminal long α-helix, four-helix bundle, and C-terminal β-sheet

domains.[10] GrpE$_{Tth}$ binds to DnaK from *T. thermophilus* HB8 (DnaK$_{Tth}$) in a 2:1 stoichiometry and accelerates ADP/ATP exchange of DnaK$_{Tth}$ up to 80,000 fold,[10] although DnaJ$_{Tth}$ does not affect ATP hydrolysis of DnaK$_{Tth}$,[10,11] forming a large 300 kDa complex composed of trimers of DnaK$_{Tth}$, DnaJ$_{Tth}$, and the assembly factor DafA.[12] Further, the two-step thermal transition observed in the DSC measurement has suggested that GrpE$_{Tth}$ has the ability to work as a thermosensor of the DnaK$_{Tth}$ system.[8] Intriguingly, GrpE$_{Tth}$ can heterologously interact with DnaK$_{Eco}$ and accelerate the nucleotide release from DnaK$_{Eco}$ with less efficiency than the homologous complexes, GrpE$_{Tth}$-DnaK$_{Tth}$ and GrpE$_{Eco}$-DnaK$_{Eco}$,[10] despite the low-level sequence identity between the GrpE proteins from these two species (26%). Therefore, it has been expected that the fundamental mechanism of the nucleotide exchange reaction for DnaK by GrpE is sufficiently conserved between the mesophilic and thermophilic DnaK systems.[10]

While GrpE$_{Eco}$ and GrpE$_{Tth}$ have functional similarity, as described above, they also show significant differences in thermal stability and temperature-dependent conformational changes, which are tightly correlated with the optimal growth temperature of each organism. The first part of the temperature-induced structural transition of GrpE$_{Eco}$ has been attributed to the unfolding of the N-terminal long paired helices,[13] which is linked to the destabilization of the β-sheet domain.[14] In the case of GrpE$_{Tth}$, the lower-temperature transition with a midpoint at 90°C has been alternatively ascribed to the unfolding of the C-terminal β-sheet

domain, not the N-terminal helices.[8] Meanwhile, the second transition (at 75-80°C in

GrpE$_{Eco}$[7] and at 100-105°C in GrpE$_{Tth}$[8]) has been considered to be responsible for the

irreversible dissociation of the GrpE dimer in both species.[8,13,14] Structural information on

GrpE$_{Tth}$ will therefore play a key role in informing the discussion about its thermostability

and the structural mechanisms involved in its functions. Here we report the crystal structure

of GrpE$_{Tth}$ and a novel structural basis for its thermosensing action.

Results and Discussion

Overall structure of GrpE$_{Tth}$ and comparison with GrpE$_{Eco}$

The crystal structure of GrpE$_{Tth}$ expressed in *E. coli* was determined at 3.23 Å resolution using the single-wavelength anomalous dispersion (SAD) technique (Figure 1a). Surprisingly, despite the large cell volume (~210^3 Å^3), only two GrpE$_{Tth}$ molecules forming a homodimer exist in a crystallographic asymmetric unit with a high solvent content (87%). The GrpE$_{Tth}$ dimer adopts a flat and sea angel (clione)-like shape composed of three domains in a protomer (the N-terminal long α-helix, central four-helix bundle, and C-terminal β-sheet domains), as found in the structure of GrpE$_{Eco}$ (Figure 1b).[6] The structural similarity between these two GrpE proteins expected previously[8,10] was corroborated by the results of this study as follows (see Figures 1 and 2).

Superimposition of each domain structure between two GrpE structures results in rmsd values of 3.7 Å (47 Cα), 1.1 Å (41 Cα), and 1.5 Å (55 Cα) for Cα atoms of the long α-helix, four-helix bundle, and β-sheet domains, respectively (Figure 1d). In this superimposition, the topological conversion for GrpE$_{Eco}$, described in the next section in detail, was taken into consideration. These values for the structural comparison were closely correlated with the degree of amino acid sequence identity (22%, 33%, and 31%, respectively). As the C-terminal β-sheet domain of GrpE$_{Eco}$ is mainly responsible for the interaction with DnaK$_{Eco}$,[6] the remarkably similar shape of the β-sheet domain of these two GrpE proteins is

thought to contribute to the functional complementarity of GrpE$_{Tth}$ with the heterogeneous DnaK$_{Eco}$ system.[10]

While the long α-helix domain of GrpE$_{Eco}$ did not form a canonical coiled-coil structure and the N-terminal 33 residues were disordered in the crystal structure,[6] the typical coiled-coil was observed in the corresponding region of GrpE$_{Tth}$. A major reason for this difference may have been the sequence diversity of the long α-helix domain, which is supported by the lower sequence identity of this domain (22%) compared to that of the other domains. GrpE$_{Tth}$ has the almost complete i+3, i+4 heptad repeat of hydrophobic residues from the N-terminus, and the N-terminal coiled-coil is also predicted by the COILS server,[15] whereas GrpE$_{Eco}$ contains an imperfect amino acid sequence for the coiled-coil formation (Figure 2).

The α-helix domain of GrpE$_{Tth}$ has a relatively higher mean B-factor value (~198 Å^2) than that of the other domains (~73 Å^2), suggesting the structural flexibility of this domain. Despite the conformational fluctuation, we could construct the GrpE$_{Tth}$ model from the vicinity of the N-termini because the N-terminal ~20 residues of the GrpE$_{Tth}$ dimer contact other N-termini of GrpE$_{Tth}$ molecules from an adjacent crystallographic asymmetric unit and the conformations of the N-terminal regions are therefore stabilized to some extent each other in the crystal.

Comparison of topology between GrpE$_{Tth}$ and GrpE$_{Eco}$

Although both the GrpE$_{Tth}$ and GrpE$_{Eco}$ dimers have similar overall structures, we found a difference in the protein topology between the two dimer formations. For the sake of clarity, we designated the long α-helix including α1 and α2 (Figure 2) as αA (αA'), α3 as αB (αB'), and the β-sheet domain as β (β') (see diagrams in Figure 1). As for the GrpE$_{Eco}$ structure from the database (PDB ID: **1DKG**), a linker inside of the four-helix bundle domain connects αA' and αB (or αA and αB'), resulting in an αA'-αB-β (αA-αB'-β') linkage (Figure 1b). Therefore, the two subunits of the GrpE$_{Eco}$ dimer were classified as protomers proximal and distal to DnaK$_{Eco}$ that bound to GrpE$_{Eco}$ in a 1:2 stoichiometry (Figure 1b).[6] This classification was made by Harrison *et al.*, who built their GrpE$_{Eco}$ model based on the discontinuous and weak electron density at the linker region in the four-helix bundle domain.[6] In contrast to this GrpE$_{Eco}$ model (here designated topology A), the corresponding linker of GrpE$_{Tth}$ alternatively connects αA and αB (αA' and αB'; here designated topology B) (Figure 1a), which is unambiguously supported by the explicitly observed experimental electron density in this region (Figure 3). Thus, we investigated whether the previously reported linker connectivity of GrpE$_{Eco}$[6] was reasonable from a structural viewpoint. The dimerization surface is mainly constructed of the four-helix bundle domains in both quaternary structures, and 4400 Å^2 or 5800 Å^2 of surface area is buried upon dimer formation in topologies A and B, respectively. Furthermore, the distributions of hydrophobic residues and electrostatic

potential maps also indicate that topology B can lead to stronger intersubunit interaction than topology A (Figure 4 and Table 1). Since a previously reported DSC experiment for GrpE$_{Eco}$ in which the temperature of the GrpE$_{Eco}$ solution was elevated beyond the normal growth conditions showed that the unfolding of the long α-helix domain precedes the dissociation of the GrpE$_{Eco}$ dimer,[13] strong interactions at the dimer interface are considered to be necessary for conforming with the biological properties. In all cases, topology B has more favorable structural features than topology A. Therefore, topology B is suggested to be the correct conformation for GrpE$_{Eco}$, as seen in GrpE$_{Tth}$, and a modified GrpE$_{Eco}$ structure adopting topology B (here designated as GrpE$_{Eco}$*), in which the chain assignments for the 116-197 residues were interconverted to their counterparts, was hereinafter used as the GrpE$_{Eco}$ model. We think that the poor electron density of the GrpE$_{Eco}$ linker[6] is insufficient for proper linkage of the polypeptide chains. However, we cannot completely exclude the possibility that topology A is the adequate conformation for GrpE$_{Eco}$, and that GrpE proteins have structural diversity in their functional shapes, as suggested previously.[16]

Thermal stability of GrpE$_{Tth}$

The optimal growth temperature of *T. thermophilus* (70-75°C) is at least 30° higher than that of *E. coli* (37°C). Comparison of the amino acid composition reveals that GrpE$_{Tth}$ has essential features to acquire enhanced thermotolerance relative to GrpE$_{Eco}$ (Table 2). Notably,

the proportion of charged polar residues of GrpE$_{Tth}$ (41.2%) is significantly greater than that

of GrpE$_{Eco}$ (33.5%), especially in the case of the residues glutamate (17.5% *versus* 13.2% for

GrpE$_{Tth}$ and GrpE$_{Eco}$, respectively) and arginine (10.7% *versus* 5.6%). Correspondingly, there

are fewer unionized polar residues in GrpE$_{Tth}$ (7.3%) compared to GrpE$_{Eco}$ (16.2%). In

addition, structure analysis of GrpE$_{Tth}$ also shows evidence for its intrinsic thermostability.

The unstructured loop regions inside of the four-helix bundle and β-sheet domains were

shortened by three residues each (Figure 2). The GrpE$_{Tth}$ dimer buries 6200 Å^2 of the

monomer solvent-accessible surface area, which is significantly larger than that for the

GrpE$_{Eco}$* dimer (5800 Å^2). The calculated electrostatic potential maps distinctly indicate that

the N-terminal half of the four-helix bundle (α2) includes a negatively charged patch whereas

the C-terminal half is positively charged, and also illustrate that the electrostatically charged

area of GrpE$_{Tth}$ is clearly larger than that of GrpE$_{Eco}$* (Figure 5). This electrostatic

complementarity in addition to the wide charged area would make it possible to form

extensive polar interactions at the dimerization interface of GrpE$_{Tth}$ rather than GrpE$_{Eco}$. This

is supported by the much larger number of intersubunit ionic pairs between the four-helix

bundle domains of GrpE$_{Tth}$ compared to GrpE$_{Eco}$* (8 *versus* 0; Table 1). Further, several

intrasubunit ionic pairs inside of the GrpE$_{Tth}$ β-sheet domains could serve to increase the

conformational stability of this domain even at the relatively high growth temperature of *T.*

thermophilus compared to *E. coli*. All these features generally found in thermophilic

proteins[17-19] contribute to the expression of the thermal stability of GrpE$_{Tth}$.

Localized partial unfolding at heat-shock temperatures

Far-UV CD spectra of GrpE$_{Tth}$ taken at two different temperatures, including the normal growth temperature (70°C) and the heat-shock temperature (90°C) of *T. thermophilus*, show that there is no statistically significant change upon the temperature shift from 70°C to 90°C (Figure 6 and Table 3), although the DSC data explicitly suggest a structural transition of GrpE$_{Tth}$ at 90°C.[8] These results lead us to hypothesize that GrpE$_{Tth}$ undergoes a structure alteration in the β-sheet domain, which is an "invisible" domain in CD analysis.[8] However, with respect to the temperature-induced conformational changes, we were uncertain about the idea that the entire β-sheet domain of GrpE$_{Tth}$ unfolds at heat-shock temperatures as suggested previously.[8] We therefore performed limited proteolysis experiments and subsequent matrix-assisted laser desorption/ionization time-of-flight mass spectrometry (MALDI TOF-MS) analysis for the resultant peptide fragments to investigate how much area of GrpE$_{Tth}$ unfolds by the heat shock. A thermophilic protease, metalloendopeptidase (MEP) from *Grifola frondosa*, that cleaves peptide bonds on the N-terminal side of lysine residues, was used for digestion of GrpE$_{Tth}$ at room temperature, 70°C, and 90°C with time course incubation. If the whole structure of the β-sheet domain were disrupted by the heat shock at 90°C, MEP could attack peptide bonds related to all three lysine residues (Lys143, Lys146,

and Lys170) in the β-sheet domain and then the corresponding peptide fragments would be detected as the proteolytic products at 90°C. However, no mass signals corresponding to fragments that had been digested at the Lys143 position were detected, although MEP cleaved GrpE$_{Tth}$ at the other two lysine positions (Figure 7 and Table 4). In this case, no bands corresponding to degraded peptides of GrpE$_{Tth}$ were detected under any of the temperature conditions without addition of MEP (Figure 7a). SDS-PAGE analysis (Figure 7) also shows that GrpE$_{Tth}$ was hydrolyzed by MEP at the Gly11-Lys12 bond (i.e. fragment 2 was produced) immediately even at room temperature, and also indicates that fragments 3 (12-169 residues), fragment 5 (12-145), fragment 6 (29-145), and fragment 7 (54-145) with their complementary short peptides (Fragments 9-11) were generated at 90°C rapidly and preferentially rather than at 70°C, although only fragment 4 (29-177) and a fraction of fragment 5 were detected in the 70°C products.

In order to interpret this difference in digestion patterns appropriately, we should consider the effects of the temperature shift on both MEP and GrpE$_{Tth}$. It is reported that the optimum temperature of MEP is 70°C and its activity is decreased to 20% at 90°C for 1 hour.[20] In addition, we examined temperature-dependent reaction rates of MEP by monitoring degradation of the full-length GrpE$_{Tth}$ under single-hit conditions, in which the limited proteolysis was performed at a GrpE$_{Tth}$/MEP ratio of 5000:1 for 0-120 min. Because full-length GrpE$_{Tth}$ is rapidly truncated by MEP at the N-terminal side of Lys12 even at room

temperature (generation of fragment 2), this area must be structurally flexible at 70°C and

90°C. Our experiments indicate that MEP reaction at 90°C is at least three times slower than

that at 70°C (data not shown). This reduction in MEP activity at 90°C is also found in the

results of proteolysis under mild conditions (GrpE$_{Tth}$/MEP = 1000:1), in which full-length

GrpE$_{Tth}$ significantly remains after 10 min of incubation with MEP at 90°C rather than at

70°C (Figure 7a). However, fragments 3, 5, 6, and 7 are distinctively observed even in the

10-min reaction product at 90°C and the generation of these fragments is obviously faster

than that at 70°C. These results imply that the remarkable difference in MEP digestion

patterns between 70°C and 90°C reflects a temperature-dependent conformational change of

GrpE$_{Tth}$ that is not due to increased activation of MEP. Thus, we believe that the structure of

the regions around Lys54, Lys146, and Lys170 would be easily disrupted in response to

increasing temperature to the extent that MEP could attack their peptide bonds. The fact that

structural changes at 90°C are induced mainly in the β-sheet domain is consistent with the

finding from our CD measurement. On the other hand, MEP cannot hydrolyze the

Gly142-Lys143 bond either at 70°C or at 90°C, suggesting that the area around Lys143 retain

its three-dimensional structure at 90°C and has comparatively high thermoresistance.

Considering these findings, we can deduce that the structural characteristics of GrpE$_{Tth}$ are as

follows. (1) A dozen N-terminal residues do not adopt a particular conformation even at room

temperature in aqueous solution. (2) At heat-shock temperatures, the localized partial

15

unfolding takes place around Lys54, Lys146, and Lys170, whereas the region around Lys143

keeps its conformation.

Correlation between the localized unfolding and functional deficiency of NEF

The region essential for the thermosensing action of GrpE$_{Eco}$ is assigned to within the

α-helix domain,[13] and the unfolding of this sensor domain induces destabilization of the

β-sheet domain conformation at heat-shock temperatures through linkages between the two

domains, e.g., a cation-π interaction between Phe86 and Arg183.[14] Despite the functional and

structural similarities between GrpE$_{Tth}$ and GrpE$_{Eco}$, similar interactions between the helical

domains and β-sheet domain were not observed in our GrpE$_{Tth}$ crystal structure, implying that

these domains of GrpE$_{Tth}$ are thermodynamically independent. Moreover, the N-terminal long

α-helix domain of GrpE$_{Tth}$ forms a stable coiled-coil, as described above, suggesting that this

region is no longer a thermosensor, unlike GrpE$_{Eco}$. In other words, the intrinsic structural

mechanisms for the heat-shock response of the two GrpE proteins seem to be different. To

understand the thermosensing mechanism of GrpE$_{Tth}$, we investigated the relationship

between the localized unfolding and functional deficiency of NEF. On the basis of the

conformational resemblance of GrpE proteins and a high degree of sequence identity (65%)

in DnaK proteins from *T. thermophilus* and *E. coli*, it is thought that GrpE$_{Tth}$ associates with

DnaK$_{Tth}$ in a manner similar to that seen in the crystal structure of the GrpE$_{Eco}$-DnaK$_{Eco}$

complex;[6] that is, DnaK$_{Tth}$ makes contact with GrpE$_{Tth}$ from one side (designated as the "front" side) of the GrpE dimer (Figure 8), and interaction sites are mainly found in the β-sheet domain with narrow interspersed areas in the other domains (Figures 2 and 8b). Amino acid residues in this contact face of GrpE are better conserved than those on the other side (the "back" side) between GrpE$_{Tth}$ and GrpE$_{Eco}$ (Figures 8b and 8c). In addition, the temperature-sensitive Lys54, Lys146, and Lys170, indicated by the limited proteolysis experiment, are located on this DnaK interaction interface (Figure 8d). In contrast, Lys143, at which GrpE$_{Tth}$ was not cleaved by MEP even at 90°C, forms an ion pair with Glu140 at the interface opposite the DnaK interaction interface, and all of the intrasubunit ionic pairs found in the β-sheet domain (Table 1) are located on this rigid back side (Figure 8d). Due to the postulated localized unfolding that arose in the DnaK interaction region by the heat shock, GrpE$_{Tth}$ might be structurally inadequate to interact with DnaK$_{Tth}$ and to open the nucleotide-binding pocket of DnaK$_{Tth}$ for release of ADP. Therefore, it appears that GrpE$_{Tth}$ has an insufficient structural environment to function as NEF for DnaK$_{Tth}$ at heat-shock temperatures. Consequently, we conclude that the localized and partial unfolding of GrpE$_{Tth}$, which is elicited by the heat shock and occurred at the contact area of DnaK$_{Tth}$, is a structural characteristic for the low-temperature transition in DSC and is also a structural basis for the functional deficiency of NEF at heat-shock temperatures. By virtue of the site-specified and small-scale unfolding, GrpE$_{Tth}$ would effectively become an inactive form for the nucleotide

17

exchange at heat-shock temperatures and it could be refolded and reactivated as NEF at permissive temperatures, implying that the NEF-inactivation in response to the heat shock would be structurally and functionally reversible (Figure 9).

Methods

Cloning, expression, and purification

The *grpE* gene (*TTHA1490*) from *T. thermophilus* HB8 was cloned into the *Nde*I/*Bam*HI

sites of pET-11a (Novagen, Darmstadt, Germany), and the recombinant plasmid was

transformed into *E. coli* strain BL21(DE3). Cells were grown at 37°C in LB medium

containing 100 μg/ml ampicillin, and the expression of the GrpE$_{Tth}$ protein was performed

without addition of isopropyl β-D-thiogalactopyranoside. The harvested cells were

resuspended and sonicated in lysis buffer (20 mM Tris-HCl, 50 mM NaCl, 5 mM

β-mercaptoethanol, pH 8.0). The soluble lysate was incubated at 70°C for 10 min, cooled on

ice, and centrifuged at 200,000 × *g* for 60 min at 4°C. The GrpE$_{Tth}$ protein was precipitated in

lysis buffer containing 1.5 M ammonium sulfate. The precipitant was then isolated by

centrifugation and resuspended in the lysis buffer. The solution containing GrpE$_{Tth}$ was

applied to a Resource Q column (GE Healthcare Biosciences, Tokyo, Japan) equilibrated with

20 mM Tris-HCl (pH 8.0) and then eluted with a linear gradient of NaCl. The

GrpE$_{Tth}$-containing fraction was applied to a hydroxyapatite column (Bio-Scale CHT10-I;

Bio-Rad, Tokyo, Japan) equilibrated with 10 mM sodium phosphate and 150 mM NaCl (pH

7.0) and then eluted with a sodium phosphate gradient. GrpE$_{Tth}$ was applied to a Hi-Load

16/60 Superdex 75 pg column (GE Healthcare Biosciences) equilibrated with 20 mM

Tris-HCl and 150 mM NaCl (pH 8.0) and then eluted with the same buffer. The purified

GrpE$_{Tth}$ solution was desalted and concentrated to 28.8 mg/ml in 20 mM Tris-HCl and 1 mM

DTT (pH 8.0).

Crystallization, data collection, and structure determination

Crystals of GrpE$_{Tth}$ were obtained by the hanging-drop vapor diffusion method at 20°C.

Drops of GrpE$_{Tth}$ were mixed with an equal volume of the reservoir solution containing 100

mM sodium acetate (pH 5.0) and 700 mM MgSO$_4$. For structure determination of GrpE$_{Tth}$,

isomorphous heavy-atom derivative crystals of Pt and Au were prepared by soaking in

reservoir solutions containing 10 mM potassium tetrachloroplatinate for 5 h and 10 mM

potassium dicyanoaurate for 24 h, respectively. X-ray diffraction data were collected using an

ADSC Quantum-315 detector on the BL41XU beamline at SPring-8 (Native1, Pt, and Au).

Crystals were soaked in the reservoir solution containing 25% (*v/v*) ethylene glycol and then

flash-frozen in a liquid nitrogen stream at 100 K before data collection. Native crystals for

higher-resolution data were grown under almost the same crystallization conditions described

above, except for addition of acetone at a final concentration of 1.5% (*v/v*) to the reservoir

solution. X-ray diffraction data of these crystals were collected using an ADSC Quantum-210

detector on the NW12 beamline at PF-AR (Native2). All of the data sets were processed with

the HKL-2000 program package.[21] Initial phases were calculated using Pt and Au derivative

data sets by the SAD method using SOLVE.[22] Three Pt and Au sites were successfully

determined, and an interpretable electron density map was obtained. The phase probability

distributions from derivative data sets were combined using the SIGMAA program of CCP4,[23] and then density modification was performed by RESOLVE[24] together with the native data set (Native1) at 3.75 Å resolution. Two GrpE$_{Tth}$ molecules were found in an asymmetric unit with a Matthews coefficient V_M value[25] of 9.7 Å^3/Da, corresponding to a solvent content of 87.3%. Several cycles of manual model building and computational refinement were carried out using the programs COOT[26] and CNS,[27,28] respectively, until the crystallographic R-factor equaled 23.4% (R_{free} = 24.2%) at 3.52 Å resolution. Atomic coordinates of the refined structure (Native1) were used as a model of the molecular replacement method with the program Molrep[29] to determine the phase angles of the structural factors of the Native2 crystal that gave better X-ray diffraction than the Native1 crystal. The GrpE$_{Tth}$ structure was refined to the crystallographic R and R_{free} factors of 21.8% and 23.8%, respectively, at 3.23 Å resolution. The final model was validated using the program MolProbity.[30] The statistics are summarized in Table 5. All discussion of GrpE$_{Tth}$ in this paper is based on the structure of the Native2 crystal unless otherwise noted. All figures representing GrpE structures were prepared with PyMOL.[31]

CD spectroscopy

Far-UV CD spectra were recorded with a J-805 spectropolarimeter (JASCO, Tokyo, Japan) from 250 nm to 190 nm at a scan rate of 50 nm/min, 1 nm resolution, 1 nm bandwidth, a time constant of 1.0 s, a sensitivity of 100 mdeg, and an accumulation of 10 scans. The

protein concentration was 2.5 μM in 20 mM sodium phosphate (pH 8.0), and the cuvette path length was 2 mm. Spectra of the identical GrpE$_{Tth}$ solution were measured at two discrete temperature conditions (70°C and 90°C), in which the temperature was held constant using a water bath. The secondary structure content against the mean residue ellipticity at 190-240 nm was estimated by means of the reference set by Yang.[32]

Limited proteolysis experiments

Limited proteolysis experiments were performed in 20 mM Tris-HCl (pH 8.0) by incubating GrpE$_{Tth}$ (50 μM) with metalloendopeptidase (MEP) from *G. frondosa* (Seikagaku Biobusiness Corp., Tokyo, Japan) at a GrpE$_{Tth}$/MEP ratio of 5000:1, 1000:1, or 500:1 (*w/w*). Enzymatic digestions were carried out for 0-120 min or 1-3 h at room temperature, 70°C, or 90°C, and were terminated by freezing. The digestion patterns were analyzed by SDS-PAGE.

Mass spectroscopy

A variety of MEP-digested GrpE$_{Tth}$ solutions were diluted 5-fold by 0.1% (*v/v*) trifluoroacetic acid, and a 2-μl portion of each diluted sample was mixed with an equal volume of a matrix solution containing 10 mg/ml sinapinic acid, 50% (*v/v*) acetonitrile, and 0.05% (*v/v*) trifluoroacetic acid. Two microliters of the mixtures were spotted onto a MALDI target plate and allowed to dry at room temperature (dried-droplet method). Mass spectra were acquired using a Voyager-DE PRO Biospectrometry Workstation (Applied Biosystems, Foster City, CA) in linear mode with external calibration using a ProteoMass Protein

MALDI-MS Calibration Kit (Sigma-Aldrich, St. Louis, MO).

Accession number

Coordinates and structure factors for GrpE$_{Tth}$ have been deposited in the PDB under accession code **3A6M**.

Acknowledgements

References

1. Hartl, F. U. & Hayer-Hartl, M. (2002). Molecular chaperones in the cytosol: from nascent chain to folded protein. *Science* **295**, 1852-1858.

2. Bukau, B., Weissman, J. & Horwich, A. (2006). Molecular chaperones and protein quality control. *Cell* **125**, 443-451.

3. Bukau, B. & Horwich, A. L. (1998). The Hsp70 and Hsp60 chaperone machines. *Cell* **92**, 351-366.

4. Packschies, L., Theyssen, H., Buchberger, A., Bukau, B., Goody, R. S. & Reinstein, J. (1997). GrpE accelerates nucleotide exchange of the molecular chaperone DnaK with an associative displacement mechanism. *Biochemistry* **36**, 3417-3422.

5. Mally, A. & Witt, S. N. (2001). GrpE accelerates peptide binding and release from the high affinity state of DnaK. *Nat. Struct. Biol.* **8**, 254-257.

6. Harrison, C. J., Hayer-Hartl, M., Di Liberto, M., Hartl, F. & Kuriyan, J. (1997). Crystal structure of the nucleotide exchange factor GrpE bound to the ATPase domain of the molecular chaperone DnaK. *Science* **276**, 431-435.

7. Grimshaw, J. P., Jelesarov, I., Schonfeld, H. J. & Christen, P. (2001). Reversible thermal transition in GrpE, the nucleotide exchange factor of the DnaK heat-shock system. *J. Biol. Chem.* **276**, 6098-6104.

8. Groemping, Y. & Reinstein, J. (2001). Folding properties of the nucleotide exchange factor GrpE from *Thermus thermophilus*: GrpE is a thermosensor that mediates heat shock response. *J. Mol. Biol.* **314**, 167-178.

9. Schlee, S. & Reinstein, J. (2002). The DnaK/ClpB chaperone system from *Thermus thermophilus*. *Cell. Mol. Life Sci.* **59**, 1598-1606.

10. Groemping, Y., Klostermeier, D., Herrmann, C., Veit, T., Seidel, R. & Reinstein, J. (2001). Regulation of ATPase and chaperone cycle of DnaK from *Thermus thermophilus* by the nucleotide exchange factor GrpE. *J. Mol. Biol.* **305**, 1173-1183.

11. Klostermeier, D., Seidel, R. & Reinstein, J. (1999). The functional cycle and regulation of the *Thermus thermophilus* DnaK chaperone system. *J. Mol. Biol.* **287**, 511-525.

12. Motohashi, K., Yohda, M., Endo, I. & Yoshida, M. (1996). A novel factor required for the assembly of the DnaK and DnaJ chaperones of *Thermus thermophilus*. *J. Biol. Chem.* **271**, 17343-17348.

13. Gelinas, A. D., Langsetmo, K., Toth, J., Bethoney, K. A., Stafford, W. F. & Harrison, C. J. (2002). A structure-based interpretation of *E.coli* GrpE thermodynamic properties. *J. Mol. Biol.* **323**, 131-142.

14. Gelinas, A. D., Toth, J., Bethoney, K. A., Langsetmo, K., Stafford, W. F. & Harrison, C. J. (2003). Thermodynamic linkage in the GrpE nucleotide exchange factor, a

molecular thermosensor. *Biochemistry* **42**, 9050-9059.

15. Lupas, A., Van Dyke, M. & Stock, J. (1991). Predicting coiled coils from protein sequences. *Science* **252**, 1162-1164.

16. Harrison, C. (2003). GrpE, a nucleotide exchange factor for DnaK. *Cell Stress Chaperones* **8**, 218-224.

17. Vieille, C. & Zeikus, G. J. (2001). Hyperthermophilic enzymes: sources, uses, and molecular mechanisms for thermostability. *Microbiol. Mol. Biol. Rev.* **65**, 1-43.

18. Tanaka, T., Sawano, M., Ogasahara, K., Sakaguchi, Y., Bagautdinov, B., Katoh, E., Kuroishi, C., Shinkai, A., Yokoyama, S. & Yutani, K. (2006). Hyper-thermostability of CutA1 protein, with a denaturation temperature of nearly 150 degrees C. *FEBS Lett.* **580**, 4224-4230.

19. Matsui, I. & Harata, K. (2007). Implication for buried polar contacts and ion pairs in hyperthermostable enzymes. *FEBS J.* **274**, 4012-4022.

20. Nonaka, T., Ishikawa, H., Tsumuraya, Y., Hashimoto, Y. & Dohmae, N. (1995). Characterization of a thermostable lysine-specific metalloendopeptidase from the fruiting bodies of a basidiomycete, *Grifola frondosa*. *J. Biochem.* **118**, 1014-1020.

21. Otwinowski, Z. & Minor, W. (1997). Processing of X-ray diffraction data collected in oscillation mode. *Methods Enzymol.* **276**, 307-326.

22. Terwilliger, T. C. & Berendzen, J. (1999). Automated MAD and MIR structure solution. *Acta Crystallogr., Sect. D: Biol. Crystallogr.* **55**, 849-861.

23. Collaborative Computational Project, Number 4. (1994). The CCP4 suite: programs for protein crystallography. *Acta Crystallogr., Sect. D: Biol. Crystallogr.* **50**, 760-763.

24. Terwilliger, T. C. (2000). Maximum-likelihood density modification. *Acta Crystallogr., Sect. D: Biol. Crystallogr.* **56**, 965-972.

25. Matthews, B. W. (1968). Solvent content of protein crystals. *J. Mol. Biol.* **33**, 491-497.

26. Emsley, P. & Cowtan, K. (2004). Coot: model-building tools for molecular graphics. *Acta Crystallogr., Sect. D: Biol. Crystallogr.* **60**, 2126-2132.

27. Brünger, A. T., Adams, P. D., Clore, G. M., DeLano, W. L., Gros, P., Grosse-Kunstleve, R. W., Jiang, J. S., Kuszewski, J., Nilges, M., Pannu, N. S., Read, R. J., Rice, L. M., Simonson, T. & Warren, G. L. (1998). Crystallography & NMR system: A new software suite for macromolecular structure determination. *Acta Crystallogr., Sect. D: Biol. Crystallogr.* **54**, 905-921.

28. Brunger, A. T. (2007). Version 1.2 of the Crystallography and NMR system. *Nat. Protoc.* **2**, 2728-2733.

29. Vagin, A. & Teplyakov, A. (1997). MOLREP: an Automated Program for Molecular Replacement. *J. Appl. Crystallogr.* **30**, 1022-1025.

30. Davis, I. W., Leaver-Fay, A., Chen, V. B., Block, J. N., Kapral, G. J., Wang, X.,

Murray, L. W., Arendall, W. B., 3rd, Snoeyink, J., Richardson, J. S. & Richardson, D. C. (2007). MolProbity: all-atom contacts and structure validation for proteins and nucleic acids. *Nucleic Acids Res.* **35**, W375-383.

31. DeLano, W. L. (2002). The PyMOL Molecular Graphics System, DeLano Scientific, Palo Alto, CA.

32. Yang, J. T., Wu, C. S. & Martinez, H. M. (1986). Calculation of protein conformation from circular dichroism. *Methods Enzymol.* **130**, 208-269.

33. Kabsch, W. & Sander, C. (1983). Dictionary of protein secondary structure: pattern recognition of hydrogen-bonded and geometrical features. *Biopolymers* **22**, 2577-2637.

Figure 1.

Structural comparisons of GrpE$_{Tth}$ with GrpE$_{Eco}$. Overall architectures of (a) GrpE$_{Tth}$ and (b)

GrpE$_{Eco}$ (extracted from the PDB entry, ID: **1DKG**; topology A) are illustrated in a ribbon

representation with several colors. Top views of these models are shown below. The position

of DnaK interacting with the proximal GrpE$_{Eco}$ molecule (magenta) is indicated by the dotted

circle in (b). Bottom cartoons illustrate the polypeptide-chain connectivity of GrpE proteins.

The αA (αA')-labeled circle indicates the α-helix domain (α1) and the first α-helix of the

four-helix bundle domain (α2). The αB (αB')-labeled circle represents the second α-helix of

the four-helix bundle domain (α3). The β (β')-labeled rectangle depicts the β-sheet domain.

(c) GrpE$_{Eco}$ in the topology B (GrpE$_{Eco}$*) constructed by the authors as a modification of

GrpE$_{Eco}$ is shown. The polypeptide chain assignment is altered and the new chains A and B

are colored magenta and red, respectively. The elements of the bottom cartoon are the same

as in (a) and (b). (d) Superimpositions of the domain structures are shown. GrpE$_{Tth}$ models

are colored in blue and cyan, and GrpE$_{Eco}$* models are colored in red and magenta.

Figure 2.

Amino acid sequence alignment of the GrpE proteins. Identical and homologous residues are

colored green and orange, respectively. The secondary structure elements of GrpE$_{Tth}$ and

28

GrpE$_{Eco}$ based on their crystal structures are illustrated above and below the sequences, respectively. Blue triangles indicate the characteristic MEP cleavage sites of GrpE$_{Tth}$ at 90°C. GrpE$_{Eco}$ residues interacting with DnaK$_{Eco}$ in the crystal structure of their complex are represented with red triangles.

Figure 3.

A stereo view of the initial experimental electron density map around the linker region of the four-helix bundle domain. The map is overlaid on the final GrpE$_{Tth}$ model (Native1). The color assignments are the same as Figure 1a.

Figure 4.

Comparison of the two possible topologies for the GrpE$_{Eco}$ structure. (a) Topology A, the original form of the PDB entry. (b) Topology B, the modified form as observed in the crystal structure of GrpE$_{Tth}$. Simplified diagrams, hydrophobic regions on the molecular surface, and electrostatic potential maps are drawn from the left panel, respectively. The blue and red colors on the electrostatic potential maps indicate regions of positive potential ($> +5$ kT/e) and of negative potential (< -5 kT/e) values, respectively. Only chain A, which corresponds to the magenta model in the left panel, is shown in the central and right panels.

Figure 5.

Comparison of the electrostatic interaction on the GrpE dimerization interfaces. Electrostatic

potential maps overlaid on one subunit of GrpE$_{Tth}$ and GrpE$_{Eco}$* (topology B) are shown. The

contour level was ±5 kT/e (the same as in Figure 4). The left cartoon illustrates the strong

electrostatic complementarities observed on the dimerization surface of GrpE$_{Tth}$. The

first-half helix of the four-helix bundle domain is charged negatively, and the second half is

positive.

Figure 6.

Far-UV CD spectra of GrpE$_{Tth}$. The CD spectra were measured at 70°C (continuous line), and

90°C (dotted line). Secondary structure contents from the CD spectra and from the crystal

structure were deduced using the reference set of Yang[32] and using the DSSP[33] program,

respectively, and their values are summarized in Table 3.

Figure 7.

Digestion patterns of GrpE$_{Tth}$ cleaved by metalloendopeptidase (MEP). (a) Limited

proteolysis experiments were performed at a GrpE$_{Tth}$/MEP ratio of 1000:1 for 0-120 min at

70°C or 90°C. (b) GrpE$_{Tth}$ was digested with MEP (500:1) for 1-3 hours. MEP-cleavage

products of GrpE$_{Tth}$ were separated by 18% SDS-PAGE and stained with Coomassie brilliant

blue. M represents molecular weight markers. Clear bands numbered on the gel for the reaction product were identified by TOF-MS analysis and the results are summarized in Table 4.

Figure 8.

Structural features of the interaction with DnaK. (a) GrpE$_{Eco}$ (white, surface model) interacts with DnaK$_{Eco}$ (cyan, ribbon model) in the crystal structure,[6] and the red area (the residues indicated by red triangles in Figure 2) of GrpE$_{Eco}$ is related to DnaK-binding. (b) The corresponding GrpE$_{Tth}$ residues are also colored red. (c) Identical and homologous amino acid residues between GrpE$_{Tth}$ and GrpE$_{Eco}$ are indicated in green and orange on the GrpE$_{Tth}$ structure, respectively, as in Figure 2. Residues of the expected DnaK-binding side are better conserved than those of the other side. (d) Structural features around the expected DnaK-binding region of GrpE$_{Tth}$. Expected DnaK-binding residues of GrpE$_{Tth}$ are colored red. MEP-sensitive residues (magenta, K146 and K170; red, K54) are located at or around the expected DnaK-binding area ("front" side). The predicted DnaK position is indicated by the dashed circle. Three ion pairs (yellow) were found on the distal side ("back" side) of the DnaK-binding region.

Figure 9.

Model for the localized and partial unfolding of GrpE$_{Tth}$. During the first transition at 90°C, the DnaK-binding regions in the β-sheet and α-helix domains unfold reversibly, resulting in the loss of the NEF function. The locations of the lysine residues inside the temperature-sensitive regions are indicated. This figure was made by arranging Groemping's model.[8]

Table 1.   The distribution of the ionic pairs and hydrogen bonds

	GrpE$_{Tth}$	GrpE$_{Eco}$	GrpE$_{Eco}$*
Ionic pairs (<5 Å)			
Inter-subunit	28	6	24
α-helix : α-helix	3	5	5
α-helix : four-helix	2	0	0
four-helix : four-helix	8	2	0
four-helix : β-sheet	15	0	19
Intra-subunit (chain A/B)	16/20	21/24	15/13
α-helix : α-helix	2/4	7/8	7/8
four-helix : four-helix	8/4	2/2	4/2
four-helix : β-sheet	0/0	12/14	4/3
β-sheet : β-sheet	6/12	0/0	0/0
Hydrogen bonds (<3.3 Å)			
Inter-subunit	5	2	1
α-helix : β-sheet	1	0	1
four-helix : four-helix	0	2	0
four-helix : β-sheet	4	0	0
Intra-subunit (chain A/B)	118/113	125/124	123/127
α-helix : α-helix	36/30	52/53	52/53
α-helix : four-helix	5/4	2/4	2/4
α-helix : β-sheet	0/0	1/0	0/0
four-helix : four-helix	41/45	35/36	38/35
four-helix : β-sheet	2/2	1/1	1/1
β-sheet : β-sheet	34/32	34/30	30/34

The Asp residue at the G122D substitution of GrpE$_{Eco}$ (PDB ID: **1DKG**) was replaced by the Gly residue, in which the atoms of the side chain had been removed.

The water molecules were omitted in the calculations for the number of the hydrogen bonds.

Table 2.   The amino acid composition of GrpE proteins

	GpE$_{Tth}$		GrpE$_{Eco}$		Ratio of a.a. composition
	Residues	(%)	Residues	(%)	in % (GrpE$_{Tth}$/GrpE$_{Eco}$)
Charged polar	**73**	**41.24**	**66**	**33.50**	**1.23**
Asp	10	5.65	13	6.60	0.86
Glu	31	17.51	26	13.20	1.33
Lys	11	6.21	13	6.60	0.94
Arg	19	10.73	11	5.58	1.92
His	2	1.13	3	1.52	0.74
Uncharged polar	**13**	**7.34**	**32**	**16.24**	**0.45**
Ser	2	1.13	7	3.55	0.32
Thr	1	0.56	8	4.06	0.14
Asn	3	1.69	8	4.06	0.42
Gln	4	2.26	8	4.06	0.56
Tyr	3	1.69	1	0.51	3.34
Nonpolar	**91**	**51.41**	**99**	**50.25**	**1.02**
Gly	15	8.47	8	4.06	2.09
Ala	21	11.86	24	12.18	0.97
Val	12	6.78	17	8.63	0.79
Leu	23	12.99	16	8.12	1.60
Ile	3	1.69	13	6.60	0.26
Met	3	1.69	9	4.57	0.37
Phe	7	3.95	3	1.52	2.60
Pro	7	3.95	9	4.57	0.87
Total	**177**	**100**	**197**	**100**	

Table 3.   The secondary structure fractions of GrpE$_{Tth}$

	70°C	90°C	crystal structure
α-helix	48.3%	48.0%	55.9%
β-strand	13.6%	13.4%	16.1%
turn	6.7%	7.2%	5.1%
random	31.4%	31.4%	22.9%
RMS	6.336	7.154	-

Table 4. **Identification of the peptide fragments from the limited proteolysis**

Fragments	Peptide	Measured mass	Expected mass $[M+H]^+$
1	1-177	$20,024.7 \pm 0.0$	20,027.7
2	12-177	$18,643.2 \pm 5.1$	18,644.2
3	12-169	$17,672.8 \pm 4.9$	17,673.0
4	29-177	$16,762.3 \pm 4.6$	16,763.2
5	12-145	$14,989.4 \pm 4.0$	14,988.0
6	29-145	$13,108.8 \pm 3.5$	13,107.0
7	54-145	$10,126.6 \pm 3.0$	10,125.6
8	61-145	$9,209.0 \pm 2.1$	9,209.5
9	146-177	$3,676.2 \pm 1.9$	3,675.2
10a	29-53	$2,998.6 \pm 3.9$	3,000.4
10b	146-169	$2,703.5 \pm 4.1$	2,704.2
11	12-28	$1,900.0 \pm 4.0$	1,900.1

Table 5. Data collection and refinement statistics

	Native1	Pt	Au	Native2
Data collection				
Space group	$P4_332$	$P4_332$	$P4_332$	$P4_332$
Cell dimensions				
a (Å)	208.6	209.3	208.8	210.4
X-ray source	SPring-8 BL41XU	SPring-8 BL41XU	SPring-8 BL41XU	PF AR NW12
Wavelength (Å)	1.0000	1.0719	1.0000	1.0000
Resolution (Å)[*]	50-3.52 (3.65-3.52)	50-3.75 (3.88-3.75)	50-3.83 (3.97-3.83)	50-3.23 (3.35-3.23)
Total reflections	420,060	352,483	653,532	375,571
Unique reflections	19,822	16,684	15,559	26,058
Completeness (%)[*]	100.0 (100.0)	100.0 (100.0)	100.0 (100.0)	99.8 (100.0)
$<I> / <\sigma(I)>$[*]	37.8 (11.3)	38.3 (9.2)	44.6 (15.7)	54.4 (10.8)
R_{sym}[*,†]	0.090 (0.356)	0.121 (0.352)	0.123 (0.343)	0.059 (0.307)
Phasing		SAD	SAD	
Resolution (Å)	50-3.75	50-3.81	50-3.90	
FOM after SOLVE		0.30	0.26	
FOM after RESOLVE	0.73			
Refinement				
Resolution (Å)				36.62-3.23
R_{work} / R_{free}[‡]				0.218 / 0.238
No. of atoms				
Protein / Water				2,449 / 18
Average B-factors				
Protein / Water (Å^2)				118.7 / 72.6
Rmsd bond length (Å)				0.007
Rmsd bond angles (°)				1.3
Ramachandran analysis[¶]				
Favored (%)				95.1
Outliers (%)				0.3

[*]Values in parentheses are for the highest resolution shell.

[†]$R_{sym} = \Sigma_{hkl}\Sigma_i | I_i (hkl) - <I(hkl)> | / \Sigma_{hkl}\Sigma_i I_i(hkl)$, where $I_i(hkl)$ is the ith intensity measurement of reflection hkl and $<I(hkl)>$ is the mean intensity obtained from multiple observations of symmetry-related reflections.

[‡]$R_{work} = \Sigma ||F_{obs}| - |F_{calc}|| / \Sigma |F_{obs}|$. R_{free} is the same as R_{work}, but for 5% subset of all reflections that were never used in crystallographic refinement.
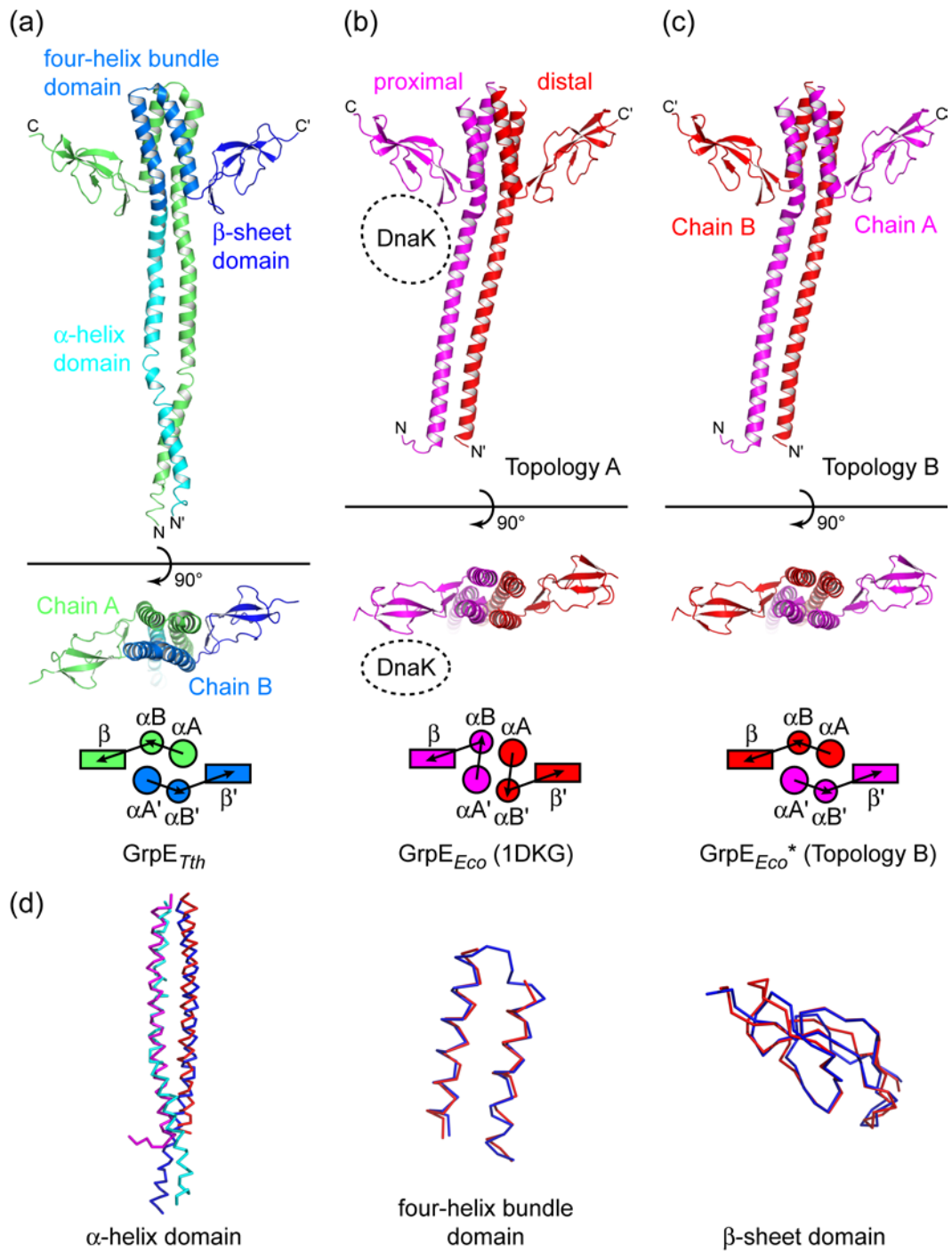
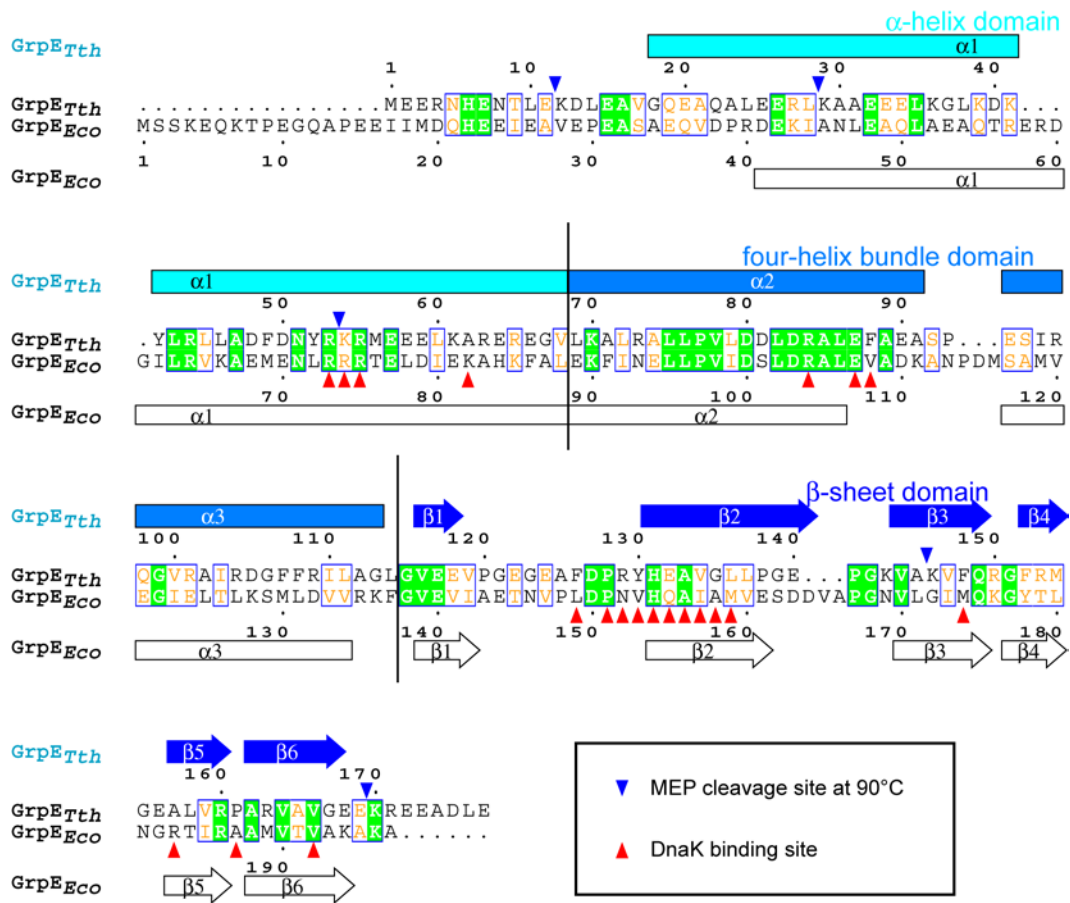[¶]Calculated by MolProbity.

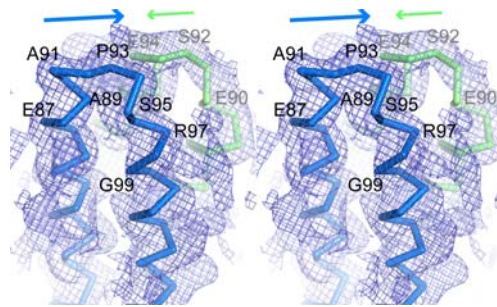Figure 1 Nakamura *et al.*

Figure 2 Nakamura *et al.*

Figure 3 Nakamura *et al.*

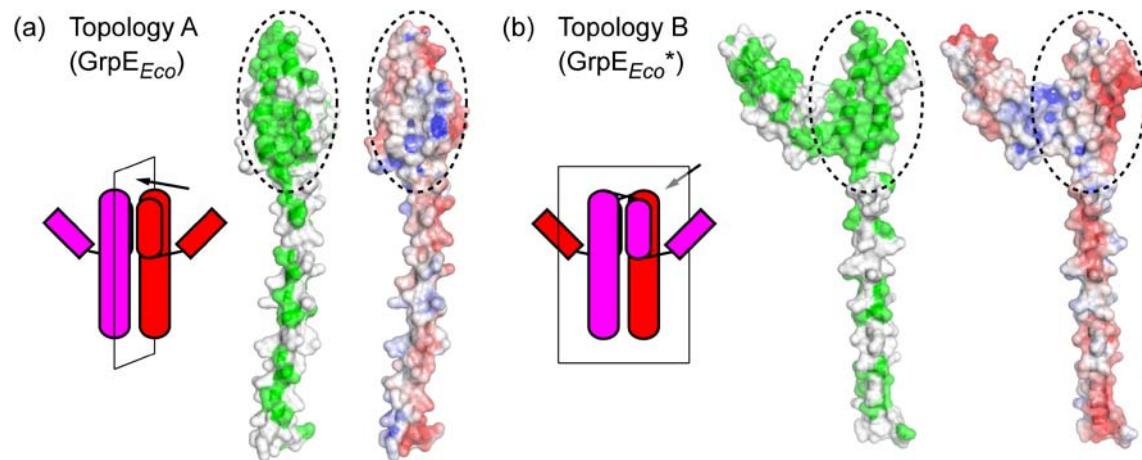(a) Topology A (GrpE$_{Eco}$)

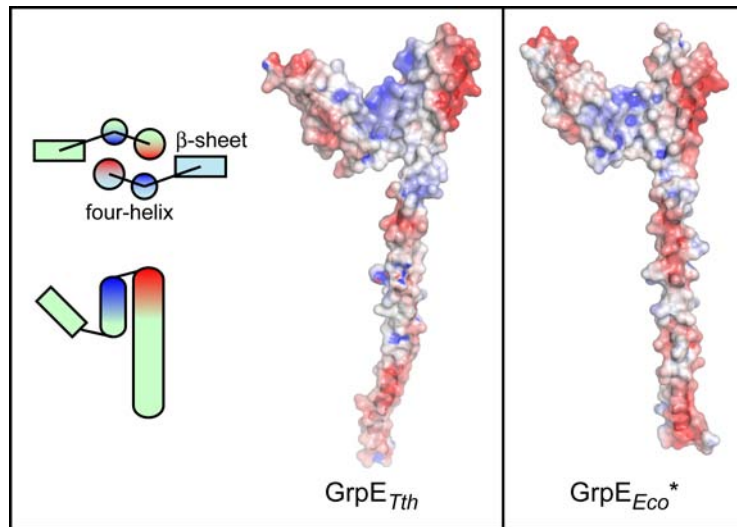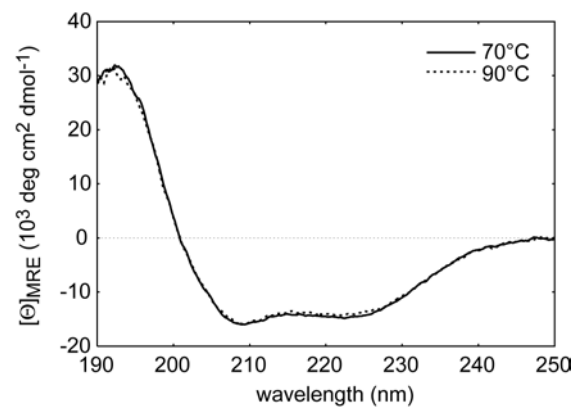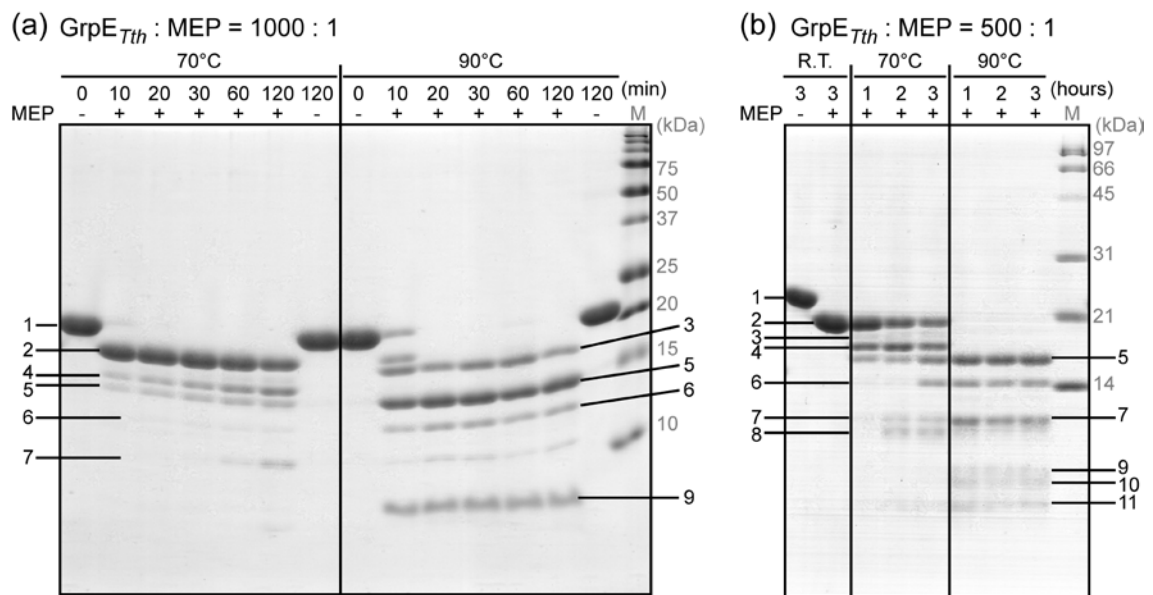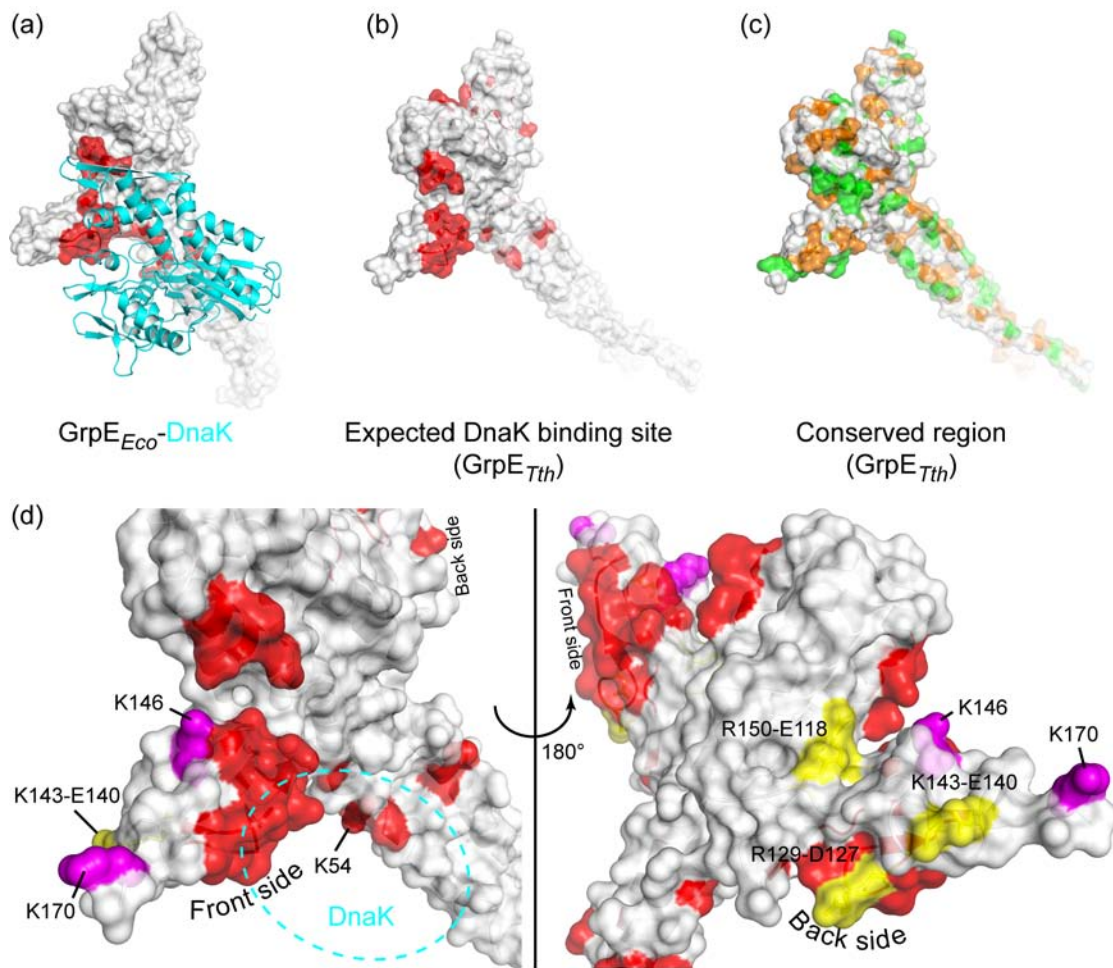(b) Topology B (GrpE$_{Eco}$*)

Figure 4 Nakamura *et al.*

Figure 5 Nakamura *et al.*
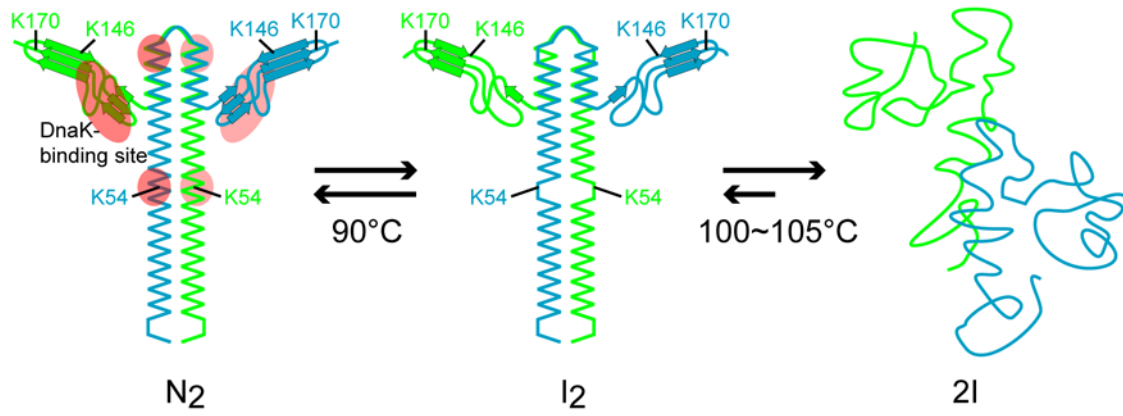
Figure 6 Nakamura *et al.*

Figure 7 Nakamura *et al.*

Figure 8 Nakamura *et al.*

Figure 9 Nakamura *et al.*